Mass Transfer in AC Electrolysis

Part III: Study of Triangular and Square-Wave Current on Rotating Electrodes

A theoretical and experimental investigation is presented for mass transfer to a rotating hemispherical electrode when direct current (DC) superimposed with symmetrical triangular- or square-wave alternating current (AC) is used for electrolysis. A film model is used for the analysis of AC concentration components. The limiting AC current density corresponding to a zero instantaneous surface concentration and the phase shift between the applied AC and the periodic potential changes are calculated and compared to the experimental studies. The experimental data agreed with the theoretical prediction to within ±8% in the regime of a dimensionless AC frequency $K = (\omega/\Omega)Sc^{1/3}$ greater than 1 and less than 180. The mass transfer behavior with the triangular and square waves is further compared to that of the sinusoidal current. It is found that for a given AC frequency and rotational speed, the limiting AC current density on the electrode decreases in the order of triangular-wave AC > sinusoidal AC > square-wave AC.

C. Y. CHENG and D.-T. CHIN

Department of Chemical Engineering
Clarkson University
Potsdam, NY 13676

SCOPE

Electrolysis using alternating current (AC) is common in pulse plating, AC corrosion, anodizing of aluminum, and charging of secondary batteries. Several AC waveforms are available for laboratory and industrial applications; they include sinusoidal, triangular, and square waves. In a previous article (Cheng and Chin, 1984a), the present authors used a film model to calculate the periodic concentration changes of a diffusing ion in laminar flow when a sinusoidal AC together with a direct current (DC) component is applied to a rotating hemisphere and a rotating disk electrode. They also presented an experimental technique (Cheng and Chin, 1984b) for the measurement of mass-transfer-limiting AC density and the phase shift between the applied AC and the resulting periodic concentration overpotential changes.

The objective of this work is to extend the previous film model and experimental measurement to AC electrolysis using symmetrical triangular- and square-wave currents. Analytical solutions were obtained for the periodic AC concentration on the surface of a rotating hemisphere electrode, and the numerical results were generated for the periodic concentration overpotential, its phase shift from the applied AC, and the limiting AC density which causes a zero concentration of the diffusing ion on the electrode surface. A gold-plated rotating hemisphere electrode and a platinum rotating disk electrode in a ferri/ferrocyanide redox electrochemical system were used for the AC mass transfer experiments over a range of AC frequencies from 10 to 1,000 Hz, and electrode rotational speeds from 300 to 3,600 rpm. The results were compared to the previous mass transfer investigations using sinusoidal current.

CONCLUSIONS AND SIGNIFICANCE

The analytical solution for the AC concentration component has been obtained with a film model for the superimposition of triangular- and square-wave AC on a rotating hemispherical electrode. The limiting AC density is found to increase with increasing AC frequency, K, and decrease with increasing DC. The phase shift between triangular-wave AC and the resulting periodic concentration overpotential increases with AC frequency and asymptotically approaches $-34 \pm 1°$. The results agreed with the experimental measurements over a range of dimensionless AC frequency K from 1 to 80. The maximum deviation was ±8% for the limiting AC density and ±9% for the phase shift measurements. A comparison with electrolysis using sinusoidal current reveals that the AC limiting current density decreases in the order of triangular-wave AC > sinusoidal AC > square-wave AC.

INTRODUCTION

Electrolysis using alternating current (AC) is common in pulse plating, AC corrosion, anodizing, battery charging, and in electrodissolution processes. AC is also used for the measurement of electrolyte conductivities, and for determination of the rate of metal corrosion using AC impedance techniques. Several waveforms are available for laboratory and industrial applications. They include sinusoidal, triangular, saw-tooth, square, asymmetric rectangular, and double-rectangular waves. Mass transfer with rectangular current, periodic pulse-reverse, and a saw-tooth current was treated by Viswanathan and Cheh (1979) and Cheh (1971a,b). Chin (1982; 1983) presented a generalized theory for AC electrolysis with asymmetric rectangular current, periodic pulse-reverse, and double-rectangular current with relaxations. He showed that very high instantaneous mass transfer rates corresponding to a peak pulse current density of 100–1,000 A/cm^2 could be attained by short current pulses at high AC frequencies. An analysis of convective mass transfer to a rotating hemispherical electrode with sinusoidal AC modulation was made by Chin (1980). In a previous article (Cheng and Chin, 1984a), the present authors used a film model to calculate the periodic concentration changes of a diffusing ion on the surface of a rotating disk electrode (RDE) and a rotating hemispherical electrode (RHE) when sinusoidal AC together with direct current (DC) was used for electrolysis. They further described an experimental setup and procedure for the measurement of the limiting AC density and the phase shift between the applied AC and the resulting periodic concentration overpotential changes (Cheng and Chin, 1984b).

The objective of this work is to extend the previous film model and experimental measurements to the superposition of symmetrical triangular- and square-wave AC onto the rotating hemisphere and rotating disk electrodes. The periodic surface concentration profile, the concentration overpotential, the limiting AC density, and the phase shift were evaluated from the theoretical model. The experiments were performed for a range of AC frequencies from 10 to 1,000 Hz and rotational speeds from 300 to 3,600 rpm ($400 < Re < 30{,}000$). The results are compared to those of sinusoidal AC modulation.

THEORETICAL ANALYSIS

The objective of this analysis is to investigate the periodic surface concentration changes on a rotating hemispherical electrode when the electrode is polarized with DC superimposed with symmetric triangular-wave or square-wave AC (Figure 1). A film model is used to simplify the solution of convective-diffusion equations.

Consider a redox reaction taking place at the surface of a RHE

$$Ox + ne^- \rightleftarrows Red \tag{1}$$

The hemispherical electrode is mounted on a supporting rod of equal radius a, and is rotating with an angular velocity, Ω, in an electrolyte of constant physical properties. The concentration of the *Red* species is much higher than that of the *Ox* species such that the concentration overpotential on the electrode surface may be solely attributed to the convective diffusion of the *Ox* species. There is an excess supporting electrolyte such that the migrational flux of the diffusing ion, *Ox*, may be assumed to be negligibly small. When the electrode surface is subjected to the passage of a DC i, superimposed with a periodic AC $\tilde{i}$, the concentration of *Ox* species may be expressed as the sum of a steady-state DC concentration component, $\overline{C}$, and a fluctuating AC concentration component, $\tilde{C}$.

The problem of the steady-state DC concentration $\overline{C}$ on the RHE has been previously treated by the present authors (Chin, 1971; Cheng and Chin 1984a). At high Schmidt numbers, Sc, the steady-state DC surface concentration with a constant wall flux on the RHE may be expressed as

$$\overline{\phi}_s(\theta) = \frac{(\overline{C}_s - C_\infty)nFD}{\bar{i}}\left(\frac{\Omega}{\nu}\right)^{1/2} Sc^{1/3}$$
$$= 1.6117 + 0.2435\theta^2 \tag{2}$$

The thickness of the Nernst diffusion layer, as determined from the steady-state concentration profile, is given by

$$\delta(\theta) = \frac{C_\infty - \overline{C}_s}{\left(\frac{\partial \overline{c}}{\partial r}\right)_a} = \overline{\phi}_s\left(\frac{\Omega}{\nu}\right)^{-1/2} Sc^{-1/3} \tag{3}$$

Using the film model (Chin, 1983; Venkatesh et al., 1982; Sethi and Chin, 1984; Cheng and Chin 1984a), the differential equation and the boundary conditions for the solution of the fluctuating concentration component, $\tilde{C}$, may be given as:

$$\frac{\partial \tilde{\phi}}{\partial \tau} = \frac{1}{K}\frac{\partial^2 \tilde{\phi}}{\partial Z^2} \tag{4}$$

at

$$\left.\begin{array}{ll} \tau = 0 & \tilde{\phi} = 0 \\ Z = 0 & \dfrac{\partial \tilde{\phi}}{\partial Z} = -f(\tau) \\ Z = \delta^* & \tilde{\phi} = 0 \end{array}\right\} \tag{5}$$

where $\tilde{\phi}$ (dimensionless AC concentration component)

$$= \frac{\tilde{C}nFD}{i_p}\left(\frac{\Omega}{\nu}\right)^{1/2} Sc^{1/3} \tag{6a}$$

$$\tau \text{ (dimensionless time)} = \omega t \tag{6b}$$

$$K \text{ (dimensionless AC frequency)} = \left(\frac{\omega}{\Omega}\right) \cdot Sc^{1/3} \tag{6c}$$

Z (dimensionless distance from the electrode)

$$= (r - a)\left(\frac{\Omega}{\nu}\right)^{1/2} Sc^{1/3} \tag{6d}$$

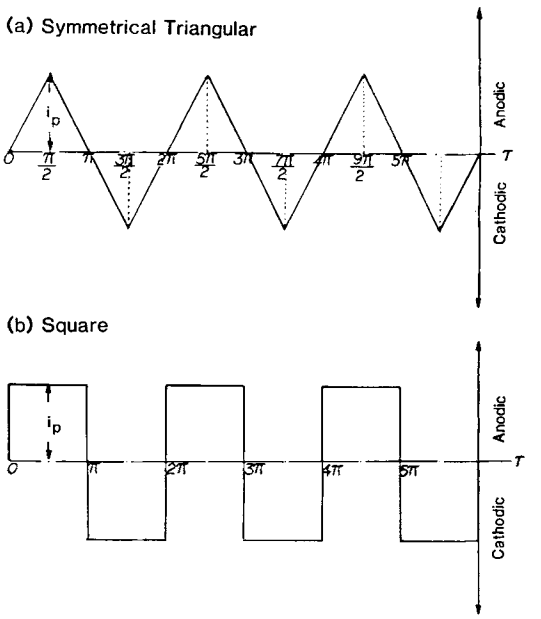

Figure 1. Symmetrical triangular-wave and square-wave AC.

$f(\tau)$ (dimensionless periodic function of AC current density)

$$= \frac{\tilde{i}}{i_p} \quad (6e)$$

δ^* (dimensionless diffusion layer thickness)

$$= \delta \left(\frac{\Omega}{\nu}\right)^{1/2} Sc^{1/3} = \bar{\phi}_s \quad (6f)$$

The quantity, i_p, in the above equations refers to the amplitude of the AC density; t is the time, ω is the AC frequency, and other quantities have their usual physical meanings (see the Notation section). The solution to Eqs. 4–5 has been obtained with the Laplace transform method (Venkatesh et al., 1982; Sethi and Chin, 1984; Chin, 1983). The result for the dimensionless AC surface concentration component can be expressed as

$$\tilde{\phi}_s(\tau) = \sum_{n=1}^{\infty} \int_0^{\tau} \frac{2f(u)}{K\delta^*} \exp\left[\frac{-\pi^2\left(n-\frac{1}{2}\right)^2}{K\delta^{*2}}(\tau-u)\right] du \quad (7)$$

Periodic AC Concentration with Triangular-Wave Current

For the symmetrical triangular-wave AC shown in Figure 1a, the dimensionless periodic function of AC, $f(\tau)$, can be expressed as

$$f(\tau) = \begin{cases} 2\tau/\pi - 4m + 4 \text{ for } (2m-2)\pi \le \tau \le \left(2m-\frac{3}{2}\right)\pi & (8a) \\ 2\tau/\pi + 4m - 2 \text{ for } \left(2m-\frac{3}{2}\right)\pi \le \tau \le \left(2m-\frac{1}{2}\right)\pi & (8b) \\ 2\tau/\pi - 4m \text{ for } \left(2m-\frac{1}{2}\right)\pi \le \tau \le 2m\pi & (8c) \end{cases}$$

where m is the number of periods ($m = 1,2,3\ldots$) in the AC waves. Substituting Eqs. 8a–8c into Eq. 7, and carrying out the integration from time zero to the Mth period, the resulting surface concentration profile can be obtained as

$$\tilde{\phi}_s\left(0 \le \gamma < \frac{1}{2}\pi\right) = \frac{2\delta^{*3}K}{\pi^5} \sum_{n=1}^{\infty} \left\{ \frac{2\exp(-\lambda_n\tau)}{\left(n-\frac{1}{2}\right)^4} + \frac{4\exp[(-\gamma-0.5\pi)\lambda_n]}{\left(n-\frac{1}{2}\right)^4[1+\exp(-\lambda_n\pi)]} + \frac{2\gamma\lambda_n - 2}{\left(n-\frac{1}{2}\right)^4} \right\} \quad (9a)$$

$$\tilde{\phi}_s\left(\frac{1}{2}\pi \le \gamma < \frac{3}{2}\pi\right) = \frac{2\delta^{*3}K}{\pi^5} \sum_{n=1}^{\infty} \left\{ \frac{2\exp(-\lambda_n\tau)}{\left(n-\frac{1}{2}\right)^4} - \frac{4\exp[(0.5\pi-\gamma)\lambda_n]}{\left(n-\frac{1}{2}\right)^4[1+\exp(-\lambda_n\pi)]} + \frac{(2\pi-2\gamma)\lambda_n + 2}{\left(n-\frac{1}{2}\right)^4} \right\} \quad (9b)$$

$$\tilde{\phi}_s\left(\frac{3}{2}\pi \le \gamma < 2\pi\right) = \frac{2\delta^{*3}K}{\pi^5} \sum_{n=1}^{\infty} \left\{ \frac{2\exp(-\lambda_n\tau)}{\left(n-\frac{1}{2}\right)^4} + \frac{4\exp[(1.5\pi-\gamma)\lambda_n]}{\left(n-\frac{1}{2}\right)^4[1+\exp(-\lambda_n\pi)]} + \frac{(2\gamma-4\pi)\lambda_n - 2}{\left(n-\frac{1}{2}\right)^4} \right\} \quad (9c)$$

Here λ_n is an eigenvalue in the infinite series

$$\lambda_n = \left(n-\frac{1}{2}\right)^2 \pi^2/\delta^{*2}K \quad (10)$$

and γ is a dimensionless time (within the Mth period) defined as

$$\gamma = \tau - 2M\pi \quad (11)$$

Eqs. 9a–9c represent a generalized solution valid for all the time domain $\tau > 0$. However, in AC electrolysis one is often interested in the steady-state periodic concentration changes. This can be obtained by letting $M \to \infty$ in Eqs. 9a–9c, and the result for the steady-state periodic AC surface concentration on the RHE is

$$\tilde{\phi}_s\left(0 \le \gamma < \frac{1}{2}\pi\right) = \frac{2\delta^{*3}K}{\pi^5} \sum_{n=1}^{\infty} \times \left\{ \frac{4\exp[(-\gamma-0.5\pi)\lambda_n)]}{\left(n-\frac{1}{2}\right)^4[1+\exp(-\lambda_n\pi)]} + \frac{2\gamma\lambda_n - 2}{\left(n-\frac{1}{2}\right)^4} \right\} \quad (\text{for } M \to \infty) \quad (12a)$$

$$\tilde{\phi}_s\left(\frac{1}{2}\pi \le \gamma < \frac{3}{2}\pi\right) = \frac{2\delta^{*3}K}{\pi^5} \sum_{n=1}^{\infty} \times \left\{ \frac{-4\exp[(0.5\pi-\gamma)\lambda_n]}{\left(n-\frac{1}{2}\right)^4[1+\exp(-\lambda_n\pi)]} + \frac{(2\pi-2\gamma)\lambda_n + 2}{\left(n-\frac{1}{2}\right)^4} \right\} \quad (\text{for } M \to \infty) \quad (12b)$$

$$\tilde{\phi}_s\left(\frac{3}{2}\pi \le \gamma < 2\pi\right) = \frac{2\delta^{*3}K}{\pi^5} \sum_{n=1}^{\infty} \times \left\{ \frac{4\exp[(1.5\pi-\gamma)\lambda_n]}{\left(n-\frac{1}{2}\right)^4[1+\exp(-\lambda_n\pi)]} + \frac{(2\gamma-4\pi)\lambda_n - 2}{\left(n-\frac{1}{2}\right)^4} \right\} \quad (\text{for } M \to \infty) \quad (12c)$$

It should be noted that there exists a recurrence formula among Eqs. 12a–12c.

$$\tilde{\phi}_s(\gamma)|_{\text{at } 0\le\gamma<1/2\pi} = -\tilde{\phi}_s(\gamma-\pi)|_{\text{at } 1/2\pi\le\gamma<3/2\pi} = \tilde{\phi}_s(\gamma-2\pi)|_{\text{at } 3/2\pi\le\gamma<2\pi} \quad (13)$$

One problem with the infinite series solutions of Eqs. 12a–12c is that the rate of convergence of the series is very slow for large values of the dimensionless AC frequency, K. To accelerate the rate of convergence, Eq. 9 can be rearranged using the imaginary Jacobian transformation (Whittaker and Watson, 1952):

$$\tilde{\phi}_s = \frac{1}{\sqrt{\pi K}} \int_0^{\tau} (\tau-u)^{-1/2} f(u) \times \left[1 + 2\sum_{n=1}^{\infty} (-1)^n \exp\left(\frac{-n^2\delta^{*2}K}{\tau-u}\right)\right] du \quad (14)$$

In the above equation, the argument of the exponential terms is $(-n^2\delta^{*2}K)/(\tau-u)$. Consequently, the rate of convergence of the

infinite series becomes faster as the values of K increases. Substituting Eqs. 8a–8c into Eq. 14 and making use of the Euler-Maclaurian summation formula (Whittaker and Watson, 1952), one obtains an alternate expression for the AC surface concentration with triangular-wave current:

$$\tilde{\phi}_s\left(0 \le \gamma < \frac{\pi}{2}\right) = \frac{1}{\sqrt{K}}\left\{\frac{16}{15}\left(\frac{\gamma}{\pi}+1.5\right)^{5/2} - \frac{8}{3}\left(\frac{\gamma}{\pi}+1.5\right)^{1.5} + \frac{4}{3}\left(\frac{\gamma}{\pi}+1.5\right)^{0.5} - \frac{16}{15}\left(\frac{\gamma}{\pi}+0.5\right)^{5/2} + \frac{8}{3}\left(\frac{\gamma}{\pi}+0.5\right)^{1.5} - \frac{4}{3}\left(\frac{\gamma}{\pi}+0.5\right)^{0.5} + \frac{2}{\pi^{3/2}}\sum_{m=1}^{M}\sum_{n=1}^{\infty}(-1)^n\left[4\mu_n^{3/2}\,\Gamma\left[-\frac{3}{2}, \frac{\mu_n}{(2m-0.5)\pi+\gamma}\right] + [(-8m+2)\pi - 4\gamma]\mu_n^{1/2}\Gamma\left[-\frac{1}{2}, \frac{\mu_n}{(2m-0.5)\pi+\gamma}\right] - 4\mu_n^{3/2}\,\Gamma\left[-\frac{3}{2}, \frac{\mu_n}{(2m-1.5)\pi+\gamma}\right] + [(8m-6)\pi + 4\gamma]\mu_n^{1/2}\,\Gamma\left[-\frac{1}{2}, \frac{\mu_n}{(2m-1.5)\pi+\gamma}\right]\right]\right\} \quad (\text{for } M \to \infty) \qquad (15a)$$

$$\tilde{\phi}_s\left(\frac{\pi}{2} \le \gamma \le \frac{3\pi}{2}\right) = \frac{1}{\sqrt{K}}\left\{\frac{16}{15}\left(\frac{\gamma}{\pi}+0.5\right)^{5/2} - \frac{8}{3}\left(\frac{\gamma}{\pi}+0.5\right)^{3/2} + \frac{4}{3}(\gamma+0.5)^{1/2} - \frac{16}{15}\left(\frac{\gamma}{\pi}-0.5\right)^{5/2} + \frac{8}{3}\left(\frac{\gamma}{\pi}-0.5\right)^{3/2} - \frac{4}{3}\left(\frac{\gamma}{\pi}-0.5\right)^{1/2} + \frac{2}{\pi^{3/2}}\sum_{m=1}^{M}\sum_{n=1}^{\infty}(-1)^n 4\mu_n^{3/2}\,\Gamma\left[-\frac{3}{2}, \frac{\mu_n}{(2m-1.5)\pi+\gamma}\right] + [(-8m+6)\pi - 4\gamma]\left[\mu_n^{1/2}\,\Gamma\left[-\frac{1}{2}, \frac{\mu_n}{(2m-1.5)\pi+\gamma}\right] - 4\mu_n^{3/2}\,\Gamma\left[-\frac{3}{2}, \frac{\mu_n}{(2m-2.5)\pi\,\mathrm{L}\,\gamma}\right] + [(8m-10)\pi + 4\gamma]\mu_n^{1/2}\,\Gamma\left[-\frac{1}{2}, \frac{\mu_n}{(2m-2.5)\pi+\gamma}\right]\right]\right\} \quad (\text{for } M \to \infty) \qquad (15b)$$

$$\tilde{\phi}_s\left(\frac{3\pi}{2} \le \gamma < 2\pi\right) = \frac{1}{\sqrt{K}}\left\{\frac{16}{15}\left(\frac{\gamma}{\pi}-0.5\right)^{5/2} - \frac{8}{3}(\gamma-0.5)^{3/2} + \frac{4}{3}(\gamma-0.5)^{1/2} - \frac{16}{15}\left(\frac{\gamma}{\pi}-1.5\right)^{5/2} + \frac{8}{3}\left(\frac{\gamma}{\pi}-1.5\right)^{3/2} - \frac{4}{3}(\gamma-1.5)^{1/2} + \frac{2}{\pi^{3/2}}\sum_{m=1}^{M}\sum_{n=1}^{\infty}(-1)^n\left[4\mu_n^{3/2}\,\Gamma\left[-\frac{3}{2}, \frac{\mu_n}{(2m-2.5)\pi+\gamma}\right] + [(-8m+10)\pi - 4\gamma]\mu_n^{1/2}\,\Gamma\left[-\frac{1}{2}, \frac{\mu_n}{(2m-2.5)\pi+\gamma}\right] - 4\mu_n^{1/2}\,\Gamma\left[-\frac{3}{2}, \frac{\mu_n}{(2m-3.5)\pi+\gamma}\right] + [(8m-14)\pi + 4\gamma]\mu_n^{1/2}\,\Gamma\left[-\frac{1}{2}, \frac{\mu_n}{(2m-3.5)\pi+\gamma}\right]\right]\right\} \quad (\text{for } M \to \infty) \qquad (15c)$$

Here $\Gamma(\alpha,x)$ is an incomplete gamma function (Abramowitz and Stegan, 1965)

$$\Gamma(\alpha,x) = \int_x^{\infty} e^{-x}x^{\alpha-1}dx \qquad (16)$$

and μ_n is an eigenvalue defined as:

$$\mu_n = n^2K\delta^{*2} \qquad (17)$$

Eqs. 15a–15b converge faster than Eqs. 9a–9c when K is larger than 100. To achieve a five-decimal accuracy at $K = 400$, for example, 4,476 terms were needed in the infinite series of Eqs. 12a–12c, compared to only four terms with Eqs. 15a–15c.

Periodic AC Concentration with Square-Wave Current

For square-wave AC, the periodic wave function $f(\tau)$ can be expressed as:

$$f(\tau) = \begin{cases} 1 & 2(m-1)\pi \le \tau < (2m-1)\pi \quad (18a) \\ -1 & (2m-1)\pi \le \tau < 2m\pi \quad (18b) \end{cases}$$

Substituting Eqs. 18a–18b into Eq. 7, simplifying the resulting equation for $M \to \infty$, and using the relation

$$\sum_{n=1}^{\infty}\frac{1}{\left(n-\frac{1}{2}\right)^2} = \frac{\pi^2}{2} \qquad (19)$$

one obtains the periodic AC surface concentration component as:

$$\tilde{\phi}_s(0 \le \gamma < \pi) = \delta^*\left\{1 - \frac{4}{\pi^2}\sum_{n=1}^{\infty}\frac{\exp(-\lambda_n\gamma)\exp(\lambda_n\pi)}{\left(n-\frac{1}{2}\right)^2[1+\exp(\lambda_n\pi)]}\right\} \quad (\text{for } M \to \infty) \qquad (19a)$$

$$\tilde{\phi}_s(\pi \le \gamma < 2\pi) = \delta^*\left\{-1 + \frac{4}{\pi^2}\sum_{n=1}^{\infty} \times \frac{\exp(-\lambda_n\gamma)\exp(2\lambda_n\pi)}{\left(n-\frac{1}{2}\right)^2[1+\exp(\lambda_n\pi)]}\right\} \quad (\text{for } M \to \infty) \qquad (19b)$$

There is a recurrence formula between Eqs. 6–19a and 6–19b:

$$\tilde{\phi}_s(\gamma)|_{\text{at } 0\le\gamma<\pi} = -\tilde{\phi}_s(\gamma-\pi)|_{\text{at } (\pi\le\gamma<2\pi)} \quad (\text{for } M \to \infty) \qquad (20)$$

A generalized mass transfer theory for AC electrolysis with asymmetrical rectangular and double-rectangular current waves has been described by Chin (1982, 1983). The present results of Eqs. 19a–19b can be also obtained from Chin's analysis by simplifying his solutions for the special case of a symmetrical rectangular current wave (i.e., a square-wave AC).

An alternate expression for the AC surface concentration at larger volumes of K may be obtained by substituting Eqs. 18a–18b into the imaginary Jacobian transform of Eq. 14. The results are:

$$\tilde{\phi}_s(0 \le \gamma < \pi) = \frac{1}{\sqrt{K}}\left\{4\left(\frac{\gamma}{\pi}\right)^{1/2} - \frac{4}{3}\left[\left(2+\frac{\gamma}{\pi}\right)^{3/2} - \left(1+\frac{\gamma}{\pi}\right)^{3/2}\right] + 2\left[\left(2+\frac{\gamma}{\pi}\right)^{1/2} - \left(1+\frac{\gamma}{\pi}\right)^{1/2}\right] - \frac{1}{3}\left[\left(2+\frac{\gamma}{\pi}\right)^{-1/2} - \left(1+\frac{\gamma}{\pi}\right)^{-1/2}\right] + \frac{2}{\pi^{1/2}}\sum_{n=1}^{\infty}(-1)^n\mu_n^{1/2}\left[\Gamma\left(-\frac{1}{2}, \frac{\mu_n}{\gamma}\right)\right.$$

$$- \sum_{m=1}^{M} \left\{ \left(-2\Gamma\left[-\frac{1}{2}, \frac{\mu_n}{(2m-1)\pi+\gamma}\right] + \Gamma\left[-\frac{1}{2}, \frac{\mu_n}{(2m\pi+\gamma)}\right] + \Gamma\left[-\frac{1}{2}, \frac{\mu_n}{(2m-2\pi+\gamma)}\right]\right)\right\} \quad (\text{for } M \to \infty) \qquad (20a)$$

$$\tilde{\phi}_s(\pi \le \gamma < 2\pi) = \frac{-1}{\sqrt{K}}\left\{4\left(\frac{\gamma}{\pi}-1\right)^{1/2} - \frac{4}{3}\left[\left(1+\frac{\gamma}{\pi}\right)^{3/2} - \left(\frac{\gamma}{\pi}\right)^{3/2}\right] + 2\left[\left(1+\frac{\gamma}{\pi}\right)^{1/2} - \left(\frac{\gamma}{\pi}\right)^{1/2}\right]\right.$$

$$- \frac{1}{3}\left[\left(1+\frac{\gamma}{\pi}\right)^{-1/2} - \left(\frac{\gamma}{\pi}\right)^{-1/2}\right] + \frac{2}{\pi^{1/2}}\sum_{n=1}^{\infty}(-1)^n\mu_n^{1/2}\left[\Gamma\left(-\frac{1}{2}, \frac{\mu_n}{\gamma-\pi}\right) - \sum_{m=1}^{M}\left\{-2\Gamma\left[-\frac{1}{2}, \frac{\mu_n}{(2m\pi-2\pi+\gamma)}\right] + \Gamma\left[-\frac{1}{2}, \frac{\mu_n}{(2m\pi-\pi+\gamma)}\right] + \Gamma\left[-\frac{1}{2}, \frac{\mu_n}{(2m\pi-3\pi+\gamma)}\right]\right\}\right] \quad (\text{for } M \to \infty) \qquad (20b)$$

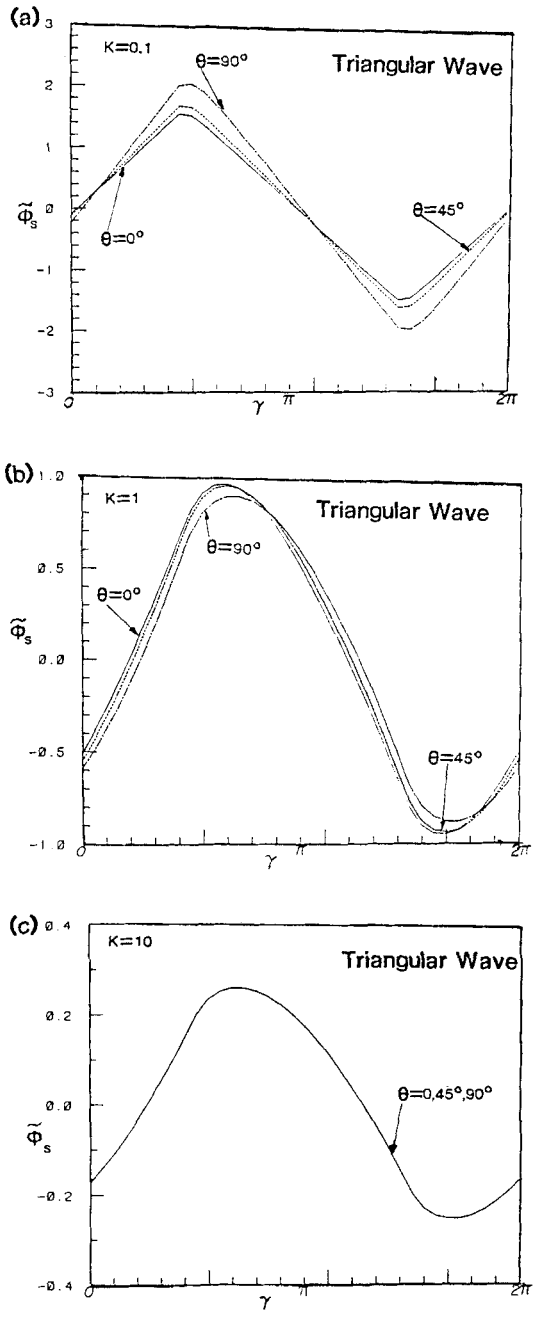

Figure 2. AC surface concentration profile for the superimposition of triangular-wave AC on the RHE.

Concentration Overpotential and Limiting AC Density

The dimensionless concentration overpotential is related to the AC and DC surface concentration components by the following relation (Cheng and Chin, 1984a):

$$\tilde{\eta}^*_{\text{conc}} = \frac{nF}{RT}\tilde{\eta}_{\text{conc}} = \ln\{[1 + \bar{i}^*\,\bar{\phi}_s + \tilde{i}_p^*\,\tilde{\phi}_s(\tau)]\} \qquad (21)$$

The limiting AC density is defined as the maximum amplitude of a superimposed AC upon which the minimum of the surface concentration wave becomes zero and $\tilde{\eta}_{\text{conc}}$ becomes infinitely large. For the rotating hemispherical electrode, the zero surface concentration occurs first at the equator ($\theta = 90°$), and the limiting AC density is calculated by the expression (Cheng and Chin, 1984a)

$$\tilde{i}^*_{p\,\text{lim}} = \frac{i_{p\,\text{lim}}}{nFDC_\infty}\left(\frac{\Omega}{\nu}\right)^{-1/2} Sc^{-1/3} = \frac{-1 - \bar{i}^*\bar{\phi}_s}{\tilde{\phi}_s(\tau_o)|_{\theta=90°}} \qquad (22)$$

where τ_o is the time corresponding to a zero instantaneous surface concentration. For the square wave, the minimum of the surface concentration profile always occurs at $\gamma = 2\pi$ (Eq. 19). For the triangular wave, the value of τ_o is a function of AC frequency, K. Also for the triangular wave, there is a phase shift, Δ_s, between the applied AC and resulting concentration overpotential. These values can be determined with numerical calculations on a digital computer.

Although the above analysis is made for the AC modulation on a rotating hemispherical electrode, the results are also applicable to the rotating disk electrode. This is so because the rotating disk electrode is a special case of the RHE which may be obtained by letting $\theta = 0°$ (Chin, 1971).

EXPERIMENTAL

To quantitatively test the theoretical analysis, a set of mass transfer experiments was made with a gold-plated rotating hemispherical electrode (1.9 cm dia.) and a platinum rotating disk electrode (0.382 cm radius). The solution used was 0.01 M $K_3Fe(CN)_6$, 0.1 M $K_4Fe(CN)_6$, and 1 N NaOH. The measurements included: the limiting DC and AC densities, the concentration overpotential (root-mean-square value), and the phase shift between the triangular-wave AC and the resulting concentration overpotential. The experimental were performed at 23° ± 1°C. The details of the experimental set-up and procedures were described in a previous report (Cheng and Chin, 1984b).

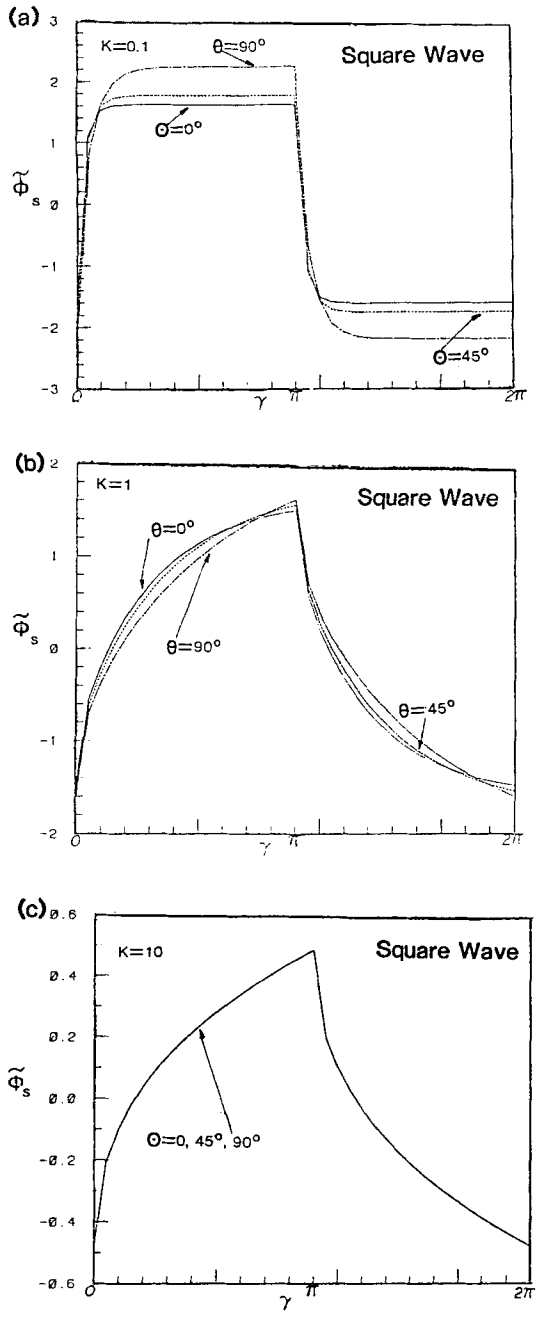

Figure 3. AC surface concentration profile for the superimposition of square-wave AC on the RHE.

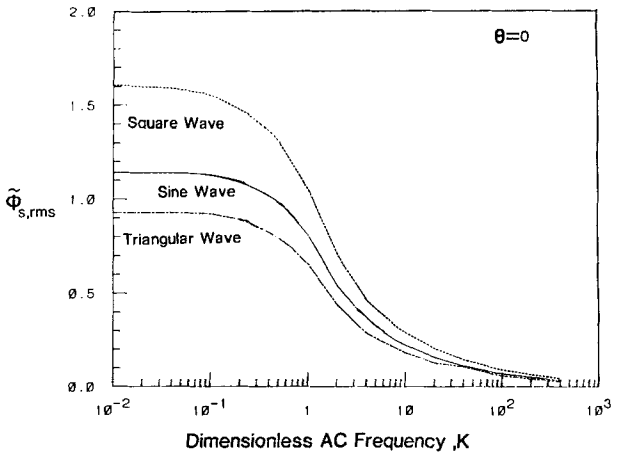

Figure 4. Root-mean-square of the dimensionless AC surface concentration component as a function of dimensionless AC frequency, *K*.

Values given are for the RHE at $\theta = 0$ for triangular, sinusoidal and square-wave AC.

RESULTS AND DISCUSSION

AC Surface Concentration

Figure 2 shows the calculated AC surface concentration wave (which is equal to the total concentration minus the DC concentration component) when a triangular-wave AC is applied to the RHE. The curves are given for three values of the dimensionless AC frequency K (0.1, 1, 10) and at three locations on the RHE surface ($\theta = 0°, 45°, 90°$). At small K values, the AC surface concentration profile behaves like a triangular wave. The profile depends on the location on the electrode surface; the maxima and minima on the concentration wave vary with θ and K. The magnitude of the periodic surface concentration decreases with increasing K and increases with increasing θ. As K increases, the AC surface concentration wave is distorted from the symmetrical triangular waveform and the profile becomes independent of the locations on the electrode surface.

Figure 3 shows the calculated AC surface concentration with the square-wave AC for the dimensionless AC frequency equal to 0.1, 1, and 10. The magnitude of $\tilde{\phi}_s$ decreases with increasing K; however, the maximum and minimum values are always located at $\gamma = \pi$ and 2π. At small K values, the profile of the AC surface concentration is dependent on the location on the hemispherical electrode; the amplitude of the AC surface concentration is greater at the equator ($\theta = 90°$) than at the pole ($\theta = 0°$). As K increases, the geometric dependence of the concentration profile diminishes. As K becomes equal to or greater than 10, the AC surface concentration at the pole becomes the same as that at the equator.

The root-mean-square (rms) of the AC surface concentration components, $\tilde{\phi}_s$, can be expressed as:

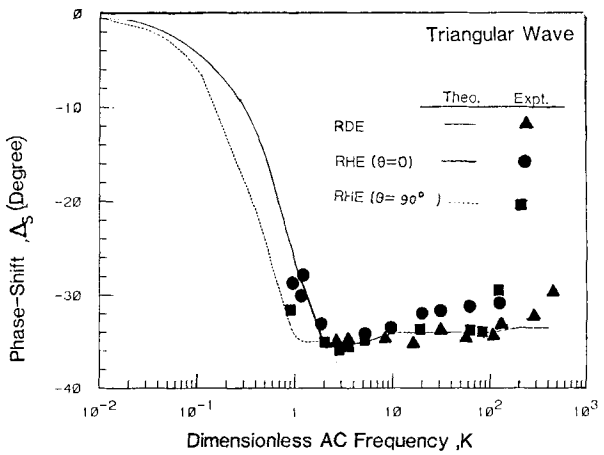

Figure 5. Phase shifts between the applied triangular AC and the concentration overpotential at the RDE and RHE at $\theta = 0°$ and 90°.

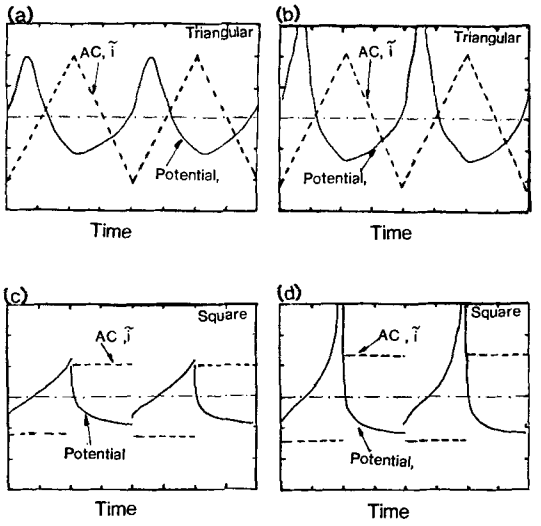

Figure 6. Oscillograms for the overpotential variations of the RDE at $K = 6$.

(a), (b): triangular-wave AC

(c), (d): square-wave AC

Time scale: 12.5 ms/div

Potential scale: 25 mV/div

Current scale: 6.25 mA/div

$$\tilde{\phi}_{s,\mathrm{rms}} = \sqrt{\frac{\int_0^{2\pi} [\tilde{\phi}(\tau)]^2 d\tau}{2\pi}} \qquad (23)$$

Figure 4 shows the rms of the dimensionless AC concentration, $\tilde{\phi}_{s,\mathrm{rms}}$ as a function of dimensionless AC frequency, K, for the triangular, square, and sinusoidal AC currents at $\theta = 0$. The curve for the sinusoidal AC modulation was calculated from the analytical results reported in a previous paper (Cheng and Chin, 1984a); it is included in the figure for the purpose of comparison. The results show that the rms of $\tilde{\phi}_s$ decreases with increasing K. Among the three waveforms, the square-wave AC produced the highest rms of the dimensionless AC surface concentration; the sinusoidal AC had an intermediate effect; and the triangular-wave AC showed the smallest effect on the concentration fluctuations on the electrode surface. For small values of K, the values of $\tilde{\phi}_{s,\mathrm{rms}}$ exhibited

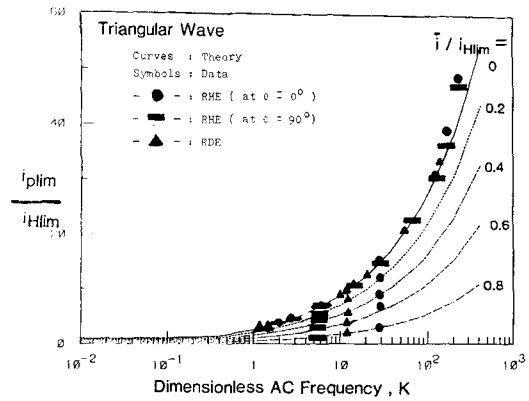

Figure 7. Limiting AC density for triangular-wave AC on the RHE as a function of AC frequency for various applied DC, $\bar{i}/i_{\mathrm{Hlim}}$.

Data obtained with the RDE are included for comparison.

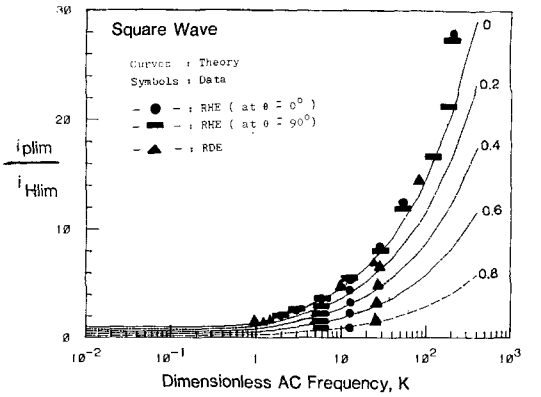

Figure 8. Limiting AC density for square-wave AC on the RHE as a function of AC frequency for various applied DC densities, $\bar{i}/i_{\mathrm{Hlim}}$.

Data obtained for the RDE are included for comparison.

a ratio equal to the ratio of the rms of the applied AC waveforms:

$$\tilde{\phi}_{s,\mathrm{rms}}(\text{square}) = \sqrt{2}\,\tilde{\phi}_{s,\mathrm{rms}}(\text{sinusoidal}) = \sqrt{3}\,\tilde{\phi}_{s,\mathrm{rms}}(\text{triangular}) \quad (\text{as } K \to 0) \qquad (24)$$

Phase Shift

Figure 5 shows the results of experimental measurements of phase shift between the triangular AC and the periodic concentration overpotential on the RDE and on the RHE at two reference locations ($\theta = 0°$ and $90°$). The geometric symbols represent the experimental data; the theoretical prediction is shown by the solid ($\theta = 0°$) and dashed ($\theta = 90°$) curves. The results indicate that the phase shift is independent of θ as K becomes larger than 2. The theoretical calculations also indicate that the phase shift asymptotically approaches $-34 \pm 1°$ as K becomes infinitely large. There is a good agreement between the theory and experimental data in the regime of $1 \leq K < 80$. The maximum deviation in this regime was ±9%. For K greater than 80, the deviation increased; this was caused by the interference of the electrical noises and the effect of ohmic overpotential at large AC frequencies as discussed in Cheng and Chin (1984a,b).

Concentration Overpotential Wave and Limiting AC Density

Figure 6 shows the oscilloscope traces of the periodic concentration overpotential when the magnitude of the applied AC was in the neighborhood of the limiting AC density. The oscillograms were obtained for the superimposition of triangular AC (Figure 6a,b) and square-wave AC (Figures 6c,d) onto the RDE at $K = 6$. The solid curves represent the concentration overpotential; the dashed curves are the applied AC. In Figure 6a, the ratio of the amplitude of the AC to the limiting DC density was 4.82, which was slightly smaller than the limiting AC density of $i_{p\ \mathrm{lim}}/i_{D\ \mathrm{lim}} = 4.94$; whereas in Figure 6b the ratio was 5.03 (greater than the limiting AC density). It can be observed that there was a large change in the amplitude of the concentration overpotential between Figures 6a and 6b. Figures 6c,d show the potential changes for square-wave AC superimposition. In Figures 6c,d the ratios of the amplitude of square-wave AC to the limiting DC density were 2.4 and 2.8, respectively. Again, there was a sudden increase in the peak of the concentration overpotential as the AC approaches the limiting AC density of $i_{p\ \mathrm{lim}}/i_{D\mathrm{lim}} = 2.6$. Thus, by gradually increasing the magnitude of the superimposed AC from the AC signal generator and observing the sudden jump in the concentration overpotential wave on the oscilloscope, one is able to determine

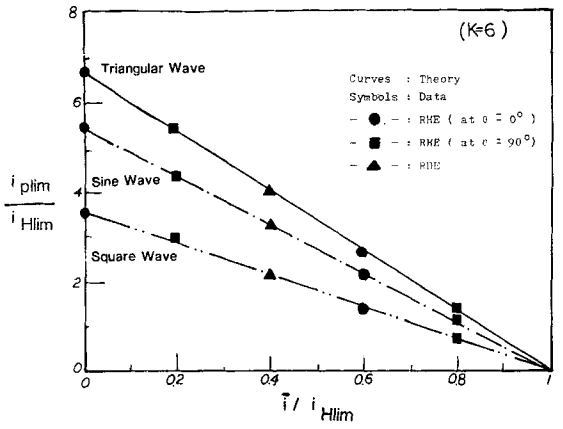

Figure 9. Limiting AC density as a function of applied DC, $\bar{i}$, for triangular, sinusoidal, and square-wave AC at $K = 6$.

$i_{p\ \mathrm{lim}}$ from the experimental measurement. The above technique was further checked by plotting the rms of the periodic concentration overpotential vs. the amplitude of applied AC. The curve in the plot exhibited two linear regions near $i_{p\ \mathrm{lim}}$ and the interception of the two lines could be taken as the limiting AC density (Cheng and Chin, 1984b). The two methods agreed with each other to within ±2%.

The limiting AC density on the RHE for the triangular- and square-wave AC superimposition are given in Figures 7 and 8, respectively. In these figures, the limiting AC density is normalized by the average limiting DC density on the RHE, $i_{H\ \mathrm{lim}}$, and is plotted against the dimensionless AC frequency K for a range of DC, $\bar{i}/i_{H\ \mathrm{lim}}$ from 0 to 0.8. The theoretical predictions are given as the curves and the geometrical symbols represent the experimental data. The results indicate that the limiting AC density increases with increasing K and decreases with increasing DC, $\bar{i}$. The experimental data agreed with the theoretical calculations to within ±5% for the triangular-wave AC ($K \leq 180$) and ±8% for the square-wave AC ($K \leq 180$).

The data shown in Figures 7 and 8 for $K = 6$ are replotted in Figure 9. For comparison, the previous theoretical prediction and experimental data for the sinusoidal AC (Cheng and Chin, 1984b) are also plotted in the figure. The limiting AC density decreased with increasing DC and became zero when DC was equal to the limiting DC density on the electrode. The values of the limiting AC density decreases according to the order:

$$i_{p\ \mathrm{lim}}(\mathrm{triangular}) > i_{p\ \mathrm{lim}}(\mathrm{sinusoidal}) > i_{p\ \mathrm{lim}}(\mathrm{square}) \quad (25)$$

This is because the square-wave AC causes the highest surface concentration fluctuation, as described in Figure 4.

ACKNOWLEDGMENT

Acknowledgment is made to the Donors of Petroleum Research Fund, administered by the American Chemical Society, for support of this research.

NOTATION

a = radius of hemisphere electrode, m
C = concentration of reacting species, kmol/m^3
$\bar{C}$ = DC concentration component, kmol/m^3
$\tilde{C}$ = AC concentration component, kmol/m^3
C_s = surface concentration of reacting species, kmol/m^3
C_∞ = bulk concentration of reacting species, kmol/m^3
D = diffusivity, m^2/s
$f(\tau)$ = dimensionless periodic function of AC current density in Eq. 6e
F = Faraday's constant, 9.65×10^7 C/k equiv.
i = applied current density, A/m^2
$\bar{i}$ = applied DC density, A/m^2
$\tilde{i}$ = applied AC density, A/m^2
i^* = dimensionless DC density, defined as $\dfrac{\bar{i}}{nFDC}\left(\dfrac{\Omega}{\nu}\right)^{-1/2} Sc^{-1/3}$
$i_{D\ \mathrm{lim}}$ = limiting DC density at the RDE, A/m^2
$i_{H\ \mathrm{lim}}$ = limiting DC density at the RHE, A/m^2
i_p = amplitude of AC density, A/m^2
i_p^* = dimensionless amplitude of AC density, defined as $\dfrac{i_p}{nFDC}\left(\dfrac{\Omega}{\nu}\right)^{-1/2} Sc^{-1/3}$
$i_{p\ \mathrm{lim}}$ = limiting AC density, A/m^2
$i^*_{p\ \mathrm{lim}}$ = dimensionless limiting AC density
K = dimensionless AC frequency, defined in Eq. 6c
m = number of periods, dimensionless
M = total number of periods, dimensionless
n = number of electrons, k equiv./kmol
n = number of terms in finite series, dimensionless
r = radial component, m
R = gas constant, 8.314×10^3 J/kmol·K
Re = Reynolds number, dimensionless, $\left(Re = \dfrac{a^2\Omega}{\nu}\right)$
Sc = Schmidt number, dimensionless, $\left(Sc = \dfrac{\nu}{D}\right)$
t = time, s
t_o = time at which the surface concentration becomes zero, s
T = temperature, K
Z = dimensionless distance from the electrode surface, defined in Eq. 6d

Greek Letters

γ = dimensionless time within the Mth period in Eq. 11
$\Gamma(\alpha,x)$ = incomplete gamma function in Eq. 16
δ = Nernst diffusion layer thickness, m
δ^* = dimensionless Nernst diffusion layer thickness, defined in Eq. 6f
Δ_s = phase shift between i and $\tilde{\phi}_s$ rad
η_{conc} = concentration overpotential, V
η^*_{conc} = dimensionless concentration overpotential, defined in Eq. 21
$\tilde{\eta}^*_{\mathrm{conc,rms}}$ = rms of $\tilde{\eta}^*_{\mathrm{conc}}$
θ = meridional coordinate of RHE, rad
λ_n = eigenvalue in Eq. 10
μ_n = eigenvalue in Eq. 17
ν = kinematic viscosity, m^2/s
τ = dimensionless time, defined in Eq. 6b
τ_o = dimensionless time at zero surface concentration
$\bar{\phi}_s$ = dimensionless DC surface concentration compo-

nent, defined in Eq. 2

$\tilde{\phi}_s$ = dimensionless AC surface concentration component, defined in Eq. 6a

$\tilde{\phi}_{s,\mathrm{rms}}$ = rms of $\tilde{\phi}_s$, defined in Eq. 23

ω = AC frequency, rad/s

Ω = rotational speed, rad/s

Subscripts

D lim = limiting current at the RDE

H lim = limiting current at the RHE

lim = limiting current

p = amplitude

rms = root-mean-square

s = surface

∞ = bulk

Superscript

* = dimensionless value

Other Symbols

— = DC component

~ = AC component

LITERATURE CITED

Abramowitz, M., and I. A. Stegan, *Handbook of Mathematical Functions*, Dover, New York, 260 (1965).

Cheh, H. Y., "Electrodeposition of Gold by Pulse Current," *J. Electrochem. Soc.*, **118**, 551 (1971a).

———, "The Limiting Rate of Deposition by P-R Plating," *J. Electrochem. Soc.*, **118**, 1,132 (1971b).

Cheng, C. Y., and D.-T. Chin, "Mass Transfer in AC Electrolysis. I: Theoretical Analysis Using a Film Model for Sinusoidal Current on a Rotating Hemispherical Electrode," *AIChE J.*, 30, 757 (1984a).

———, "Mass Transfer in AC Electrolysis. II: Experimental Study with Sinusoidal Current," *AIChE J.*, **30**, 765 (1984b).

Chin, D.-T., "Convective Diffusion on a Rotating Spherical Electrode," *J. Electrochem. Soc.*, **118**, 1,438 (1971).

———, "Sinusoidal AC Modulation of a Rotating Hemispherical Electrode," *J. Electrochem. Soc.*, **127**, 2,162 (1980).

———, "Mass Transfer in Pulse Electrolysis," *Proc. Symp. Transport Process in Electrochem. System*, R. S. Yeo, T. Katan, and D.-T. Chin, Eds., Electrochem. Soc., Pennington, NJ, 21–39 (1982).

———, "Mass Transfer and Current-Potential Relation in Pulse Electrolysis," *J. Electrochem. Soc.*, **130**, 1,657 (1983).

Sethi, R., and D.-T. Chin, "Sinusoidal Voltage Modulation of a Copper Rotating Disk Electrode," *J. Electroanal. Chem.*, **160**, 79 (1984).

Venkatesh, S., M. Meyyappan, and D.-T. Chin, "Mathematical Modeling of AC Modulation of a Copper Rotating Disk Electrode in Acidic Sulfate Solution," *J. Colloid and Interface Sci.*, **85**, 216 (1982).

Viswanathan, K., and H. Y. Cheh, "Mass Transfer Aspects of Electrolysis by Periodic Currents," *J. Electrochem. Soc.*, **126**, 398 (1979).

Whittaker, F. T., and G. N. Watson, *A Course of Modern Analysis*," 4th Ed., Cambridge Univ. Press, 127–128; 491–535 (1952).

Manuscript received May 14, 1984; revision received Nov. 7 and accepted Nov. 24.